Finite Element Method Simulation of a High Speed Wound-Rotor Synchronous Machine

Huijuan Liu[1], Longya Xu[2], Mingzhu Shangguan[1]
[1] School of Electrical Engineering, Beijing Jiaotong University, Beijing, 100044, China
[2] Department of Electrical & Computer Engineering, The Ohio State University, Columbus, Ohio 43210, USA
E-mail: hiliu@bitu.edu.cn

Abstract —The paper comprehensively describes the simulation of a 1000kW/18900rpm wound-rotor synchronous machine (WRSM) by using the 2D transient finite element (FE) analysis method. The magnetic fields, the iron losses, the electromagnetic torque and the terminal characteristics of the prototype machine are investigated. The *q*-axis inductance L_q and the *d*-axis inductance L_d of the sample machine are predicted in analytical models. All studies indicate that the wound-rotor synchronous machine is potential to apply in high speed generator or motor application.

I. INTRODUCTION

Many types of electrical machines can be considered for an application to generator or motor, such as synchronous machine, induction machine and switched reluctance machine. Wound-rotor salient-pole synchronous machines are widely used in high power, high performance ac system drive applications, such as main drives in steel mills. The Wound rotor synchronous machine (WRSM) have great advantages: low cost (no PM) and three control variables (i_d, i_q and i_f) allow various optimization possibilities compared with permanent magnet (PM) machine (i_d and i_q). A judicious control of these three control variables may allow a near unity power factor. A special design of the rotor, minimizes the required field current and allows the use of a rotating transformer if a total brushless configuration is required. The flux-density level in the air gap is limited only by the quality of sheets. Beyond these advantages, it is interesting to note a significant improvement of the safety and limiting the risks of high voltages for high-speed operations. Moreover, during the generating mode, the converter can be operated in a synchronous rectifier mode, thus authorizing an increase in the efficiency and a reduction in the electromagnetic disturbances and converter losses by avoiding an operation in the pulse width modulation (PWM) mode.

In this paper, the model of the 1000kW/18900rpm WRSM is described. Then, using finite element analysis, the magnetic fields distribution, the cross saturation phenomenon, the torque and the terminal characteristics of the WRSM are presented. The *q*-axis inductance L_q and the *d*-axis inductance L_d of the prototype machine are predicted in analytical models. The results are considered accurate because the complicated geometry of the WRSM and nonlinearity of the materials are full considered. The simulation results are discussed and evidence that the WRSM presents interesting performances for high speed generator or motor applications.

II. SIMULATION RESULTS

A. The prototype Machine of WRSM

Fig. 1 gives the configuration of the sample WRSM with a single pole cross-section. This machine is designed with 4 pole-pair rotor. The primary torque is produced by the three-phase stator windings and the rotor magnetic fields, and the frequency of the stator winding determines the synchronous speed of the rotor. The stator is fed with a three-phase voltage source at 1260 Hz, and the rated speed is 18900 rpm. The rotor windings are excited with DC current. By try-and-error, the WRSM main dimensions are determined with the design specifications listed in Table 1.

TABLE I MAIN DIMENSIONS

Rated Power (kW)	1000	Rated Speed (rpm)	18900
Rated V_p (V, rms)	4809	Rated Freq. (Hz)	1260
Rated I_P (A, rms)	81.5	Pole number	8-pole
Power Factor	0.85	Stator Slots	48
Stator OD (mm)	302	Stator ID (mm)	154
Rotor OD (mm)	152.8	Stack Length (mm)	185
R_a（Ω）	0.0007	Air gap（mm）	0.6
L_d(H)	0.052	L_q(H)	0.042
X_d(Ω)	411.5	X_q(Ω)	332.3

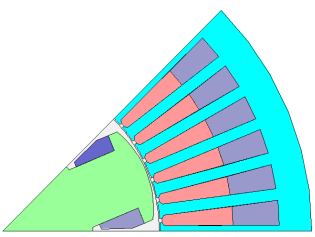

Fig. 1 Cross section of the WRSM

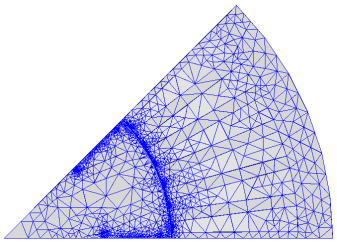

Fig. 2 Mesh division of the WRSM

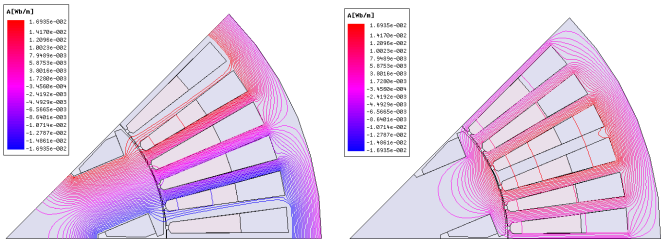

(a) d-axis excited only (b) q-axis excited only

Fig. 3 Flux distribution of a WRSM

B. *No-load operation performances*

In the finite element analysis, the transient model of the sample WRSM is built directly to simulate the performance of the no-load operation mode.

The mesh division of the sample WRSM is shown in Fig. 2. When the rotor winding is excited with d-axis or q-axis DC current, the flux distribution over the cross-section of the sample WRSM is shown in Fig. 3(a) and (b) respectively.

When the WRSM operates at no-load mode, it is only the fields winding (the rotor winding) is excited with DC current at a ampere-turn , the three-phase stator windings on open circuit and the rotor is rotating at a constant speed, then the EMF will be induced in the armature windings. In these cases, the three-phase stator windings terminal voltages on open-circuit are a function of the field excitation. Fig. 4 shows the magnetizing curve of the sample WRSM while the rotor rotating at different speed, 18900rpm, 15000rpm, 12000rpm, and 9000rpm. From the no-load characteristics, we can find that the fields of the machine will get into saturation when the excitation current at 900 ampere-turn and the magnetization characteristic of the sample machine is enough fine to operate for a generator or a motor.

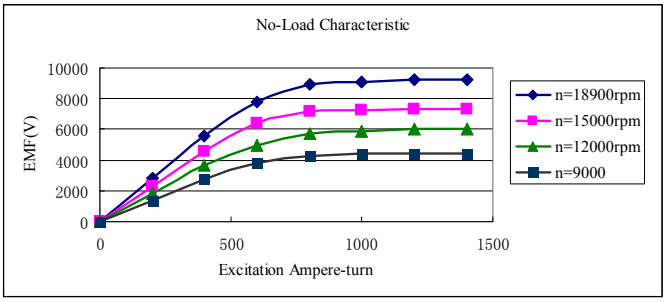

Fig. 4 No-load characteristic of the sample machine

By using FEM, we have also investigated the air-gap flux density distribution and the induced back EMF of the stator winding. Fig. 5 shows the air-gap flux density of the WRSM at no-load operation, and the waveform of the flux density is closed to sine wave. The results show that the magnetic field in the air gap is reasonable. Fig. 6 shows the calculated harmonic contents of the air-gap flux density waveform, and the features of the sinusoidal is proved clearly. Fig. 7 shows the mutual-flux linkages of the stator windings, so the sine EMF can be deduced in the three-phase stator windings as shown in Fig. 8.

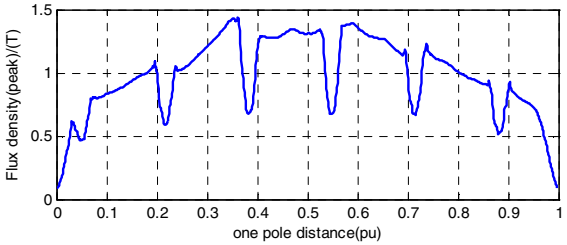

Fig. 5 Air-gap flux density at no-load operation

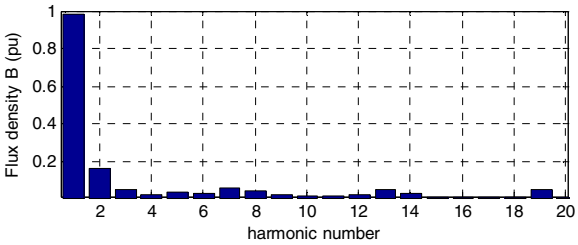

Fig. 6 Harmonic contents of the air-gap flux density

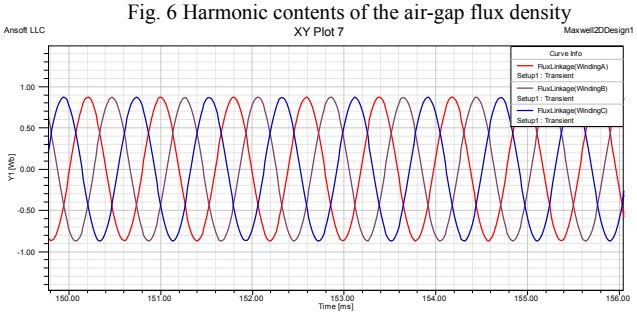

Fig. 7 Waveforms of mutual-flux linkages

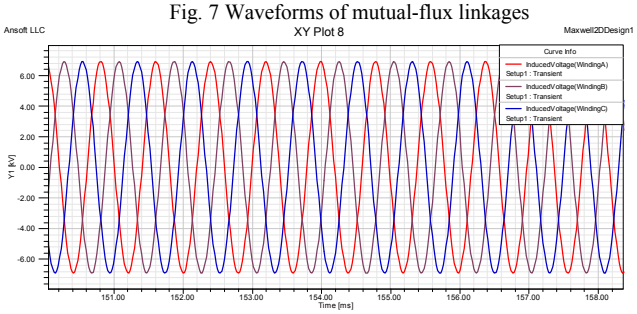

Fig. 8 Waveforms of induced voltages

C. *Calculation of the L_q and L_d*

In this section, the transient model of the sample WRSM is built directly to calculate the *q*-axis inductance L_q and the *d*-axis inductance L_d.

The calculation is conducted with the rotor rotating at 18711rpm, not the rated synchronous speed 18900rpm, and the slip is 0.01. The rotor field windings are not excited with any sources and on open circuit, while the three-phase stator windings are fed with AC current at 1260Hz, the current peak is 4A. Fig. 9 (a) and (b) show the flux linkage and the back EMF of the stator phase *A* respectively. The results show that the maximum flux linkage of phase *A* is 0.208Wb, the minimum flux linkage is 0.168Wb, the maximum back EMF of phase *A* is 1978V and the minimum back EMF is 1220V. By using flux linkage results, the L_q, L_d, X_d and X_q shown in Table I can be calculated.

L_d=0.208/4=0.052H, $X_d=\omega L_d$ =411.5Ω;

L_q=0.168/4=0.042H, $X_q=\omega L_q$ =332.3Ω.

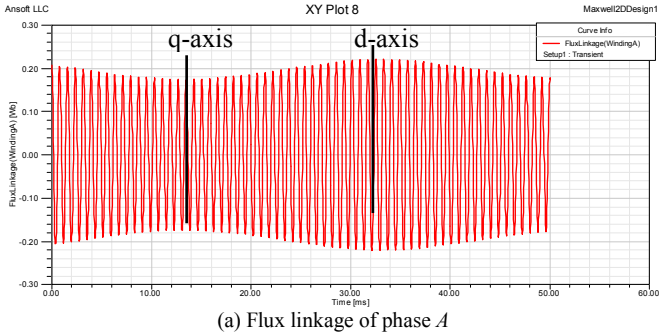

(a) Flux linkage of phase *A*

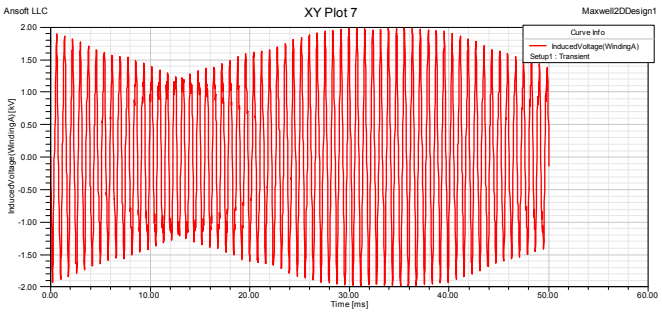

(b)EMF of phase *A*

Fig. 9 Flux linkage and EMF of the stator winding

D. Determination of the Initial Positions

In order to produce an expectative constant torque (positive or negative), the position of the rotating magnetic field in the air-gap and the rotor position should be controlled properly. In finite element analysis, it means that the initial positions of the rotor should be predetermined properly. The simulation is conducted with the rotor rotating at the rated speed while the other parts are fixed, the rotor fields winding is fed with DC current and the three-phase stator windings are imposed on a constant DC current, such as (110A, -55A, -55A). The corresponding static torque obtained is as shown in Fig. 10 which shows the torque-position curve varies sinusoidally and at any rotor angle.

If the WRSM carries no load, it will stay at its no-load equilibrium positions (0 Nm). As the load increases, the magnetic torque will go up along the torque curve to the new equilibrium position. When the load is larger than the maximum static torque (734Nm) of the torque curve, the machine will get into the unstable operation area as shown in Fig. 10.

In this paper, considering the overloading factor (1.8~2.2) of the WRSM, the rated load is designed with nearly half of the maximum static torque of the machine, namely 410 Nm. In order to analyze the full load performance of the machine, the initial position of the rotor should be at 230/4=57.5 mechanical degrees from the no-load equilibrium position. For the stator windings, since the speed of the magnetic field produced by the stator currents is synchronized with that of the rotor, the initial position should be consistent with that of the rotor.

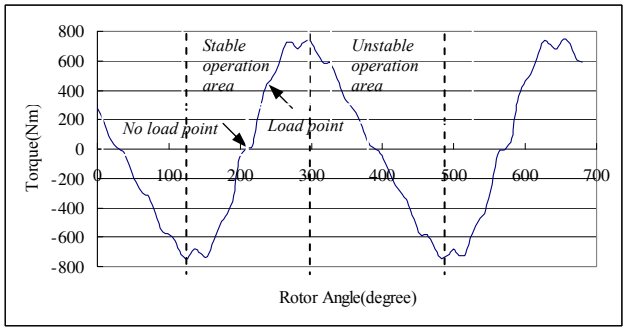

Fig. 10 Static torque performance of the sample machine

E. Loaded operation performances

The transient model of the sample WRSM is built to simulate the full load operation. The advantage of the transient simulation model is that the realistic conditions of lamination geometries, core materials, and winding connections are all considered collectively and faithfully.

The magnetic flux distribution of the sample WRSM at full load operation can be investigated when the fields winding is excited with rated DC current, and the rated three-phase sine AC voltages 4809V are imposed to the stator windings. It is important to note that once the rotor is rotating at 18900rpm, induced back EMF of 1260Hz, the speed voltages will be generated in the three-phase stator windings. Additional electromechanical energy conversion will occur in the machine. At this rated operation mode, the flux distribution over the cross-section of the sample WRSM is shown in Fig. 11(a), the flux density of the cross-section is shown in Fig. 11(b), and the part saturation phenomenon is clear. From Fig. 11(b), we can find that the average flux density and the maximum flux density in rotor core are about 1.7T and 2.1T respectively, the maximum flux density in stator are occurred at stator tooth, about 2.1T, the average flux density in stator yoke is about 0.8T to 1.6T. It is seen that the flux distribution shown in Figs. 11 is still representative for excitation of any frequency at any rotor speed.

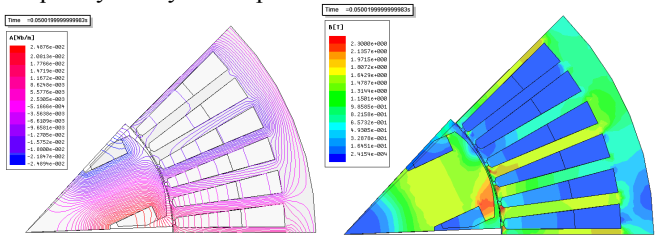

(a) Flux distribution (b) Flux density

Fig. 11 The magnetic fields features of a WRSM in loaded operation

F. Torque Capability and Efficiency

The torque capacity of the sample WRSM can be calculated using Maxwell's stress tensors in the air-gap. The full-load torque transmission of the machine simulated with FEM, as shown in Fig. 12. During the simulation, the stator windings are fed with 6800V (peak), three-phase sinusoidal voltages. The stator current of phase A is shown in Fig. 13, and the peak of the current is about 115A. The corresponding induced torque by the stator windings is about 412 Nm as shown in Fig. 11, which is used to produce the motive torque on the rotor.

The transient core loss at the full-load operation is simulated with dynamic core loss model and the core loss curves are shown in Fig. 14. The core loss is about 55kW, which are mainly induced in the stator core and rotor core.

By using the phasor diagram of the sample machine, the power angle 50.44° can be calculated.

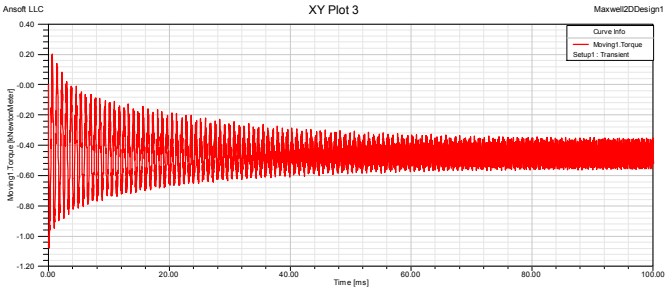

Fig. 12 Full load torque versus time

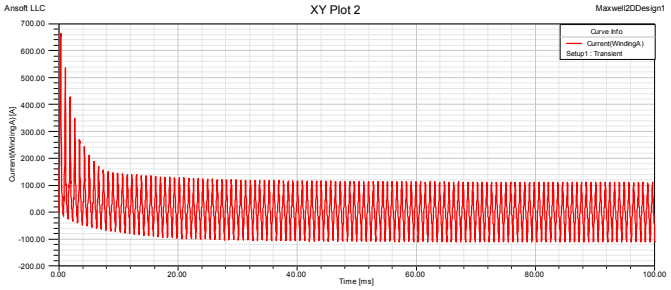

Fig. 13 Stator current of phase *A*

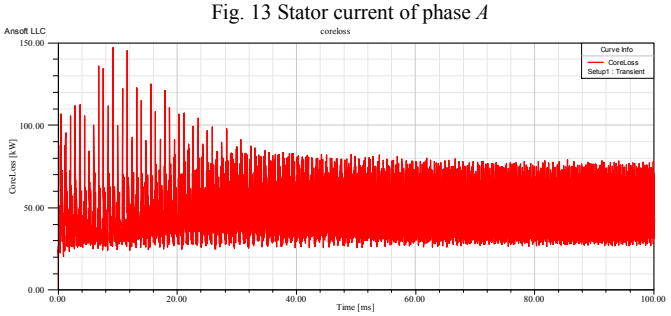

Fig. 14 Core losses at full load operation

If the initial phase angle of the three phase voltages is changed from 0 to 360 degree at step with 10 degree, during the every simulation, the peak of the voltage is 6800V; the corresponding induced torque is calculated as shown in Fig. 15. From Fig. 15, the maximum torque of the sample WRSM can achieve 720Nm at 18900rpm, and the maximum power of the machine can achieve 1424kW.

The sinusoidal torque curve shown in Fig. 15 also named as the power-angle characteristic of the synchronous machine, only the angle degrees figuring on the abscissa axis are not the power angles directly but are the initial phase angles of the phase voltage.

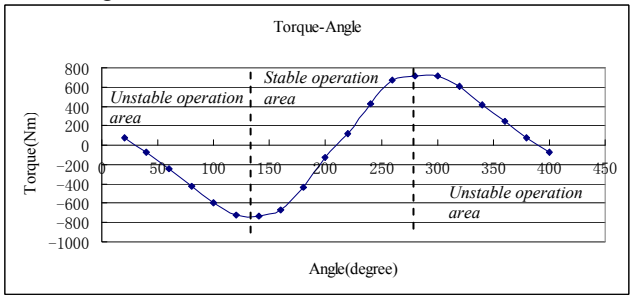

Fig. 15 Torque-angle characteristic of the sample machine

TABLE II EFFICIENCY CALCULATION

I(peak, A)	*n*(rpm)	Torque (kNm)	P_{out} （kW）	Copper losses (W)	Core losses (kW)	efficiency
115	18900	0.46	909.97	177.2	55	0.943
130	15000	0.56	879.2	200.3	33	0.964
140	13500	0.64	904.32	215.7	28	0.97
150	12000	0.72	904.32	231.1	27	0.971
160	10500	0.8	879.2	246.5	26	0.971
170	9000	0.88	828.96	261.9	25	0.97

Note that if the current phase angles of the three phases *A*, *B* and *C* are in phase with the no-load induced speed voltages of phase *A*, *B* and *C* respectively, or equivalently, orthogonal to the variation of the mutual flux linkage of phase *A*, *B* and *C* respectively**.** A maximum torque production for the given currents is expected. These show that the torque of the prototype WRSM can be controlled flexibly when appropriate control methods are applied on the system.

The torque production of a WRSM is also affected by the stator winding currents and its frequency, namely the rotor speed, when the field current is constant at certain values. Table II lists the calculation results of the sample machine operated at motor mode with different speed. The copper losses and the core losses are calculated correspondingly, but the mechanical losses are not included in efficiency calculation. During the simulation, the three-phase stator windings are supplied with constant voltage sources, the peak of the voltage is 6800V, and the voltage frequency is different in terms of the different rotor speed. The efficiency of the sample WRSM can achieve 94% at full load operation. The core loss is larger than the copper loss owing to the high frequency. The calculation results show that the efficiency of the machine can achieve higher at the lower rotor speed.

III. CONCLUSIONS

This paper focuses on the simulation performance of a prototype WRSM (1000kW/18900rpm) for generator applications. The magnetic fields distribution, the torque characteristics, the core losses, the terminal characteristics, the *q*-axis inductance L_q and the *d*-axis inductance L_d of the prototype machine are presented. The efficiency of the full load sample machine can achieve 94%. All studies show that the WRSM is potential to apply in high speed generator or motor system.

IV. REFERENCES

[1] S. Morimoto, Y. Takeda, T. Hirasa, and K. Taniguchi, ‘‘Expansion of operating limits for permanent magnet motor by current vector control considering inverter capacity,’’ IEEE Trans. Ind. Appl., vol. 26, Sept./Oct. 1990, pp. 866–871.

[2] J. Legranger and G. Friedrich, ‘‘Design of a brushless rotor supply for a wound rotor synchronous machine for integrated starter generator,’’ in Proc. IEEE VPPC [CD ROM], Sept. 2007.

[3] Friedrich, G. Comparative Study of Three Control Strategies for the Synchronous Salient Poles and Wound Rotor Machine in Automotive Application with On Board Energy Proc. of Power Electronics and Variable Speed Drives, London, UK, 26-28 Oct 1994 pp. 706-709.

[4] C. Rossi, D. Casadei, A. Pilati, M. Marano “Wound Rotor Salient Pole Synchronous Machine Drive for Electric Traction” IEEE Conference of Industry Applications, 2006. pp. 1235-1241.

[5] Chalmers, B.J. Musaba, L. Gosden, D.F. “Variable-frequency synchronous motor drives for electric vehicles”, Proc. of Industry Applications Conference, 1995. 8-12 Oct. 1995 Orlando FL USA, Volume: 1, Page(s): 717 -724.

[6] L.Chedot and G.Friedrich, “Integrated starter generator: the need for an optimal design and control approach application to a permanent magnet machine,” in *IEEE IAS Trans*, April 2007, pp. 551–559.

[7] G.Friedrich and A. Girarin, “Design, principle, constraints and optimal control of integrated starter generator,” IEEE Industry application magazine, Aug. 2009, pp. 26–34.

[8] G.Friedrich, “Experimental comparison between Wound Rotor and Permanent Magnet Synchronous machine for Integrated Starter Generator applications”, IEEE Energy Conversion Congress and Exposition (ECCE), 2010, pp. 1731–1736.

[9] Bash, M.; Pekarek, S.; Sudhoff, S.; Whitmore, J.; Frantzen, M. “A comparison of permanent magnet and wound rotor synchronous machines for portable power generation”, Power and Energy Conference at Illinois (PECI), 2010 pp: 1–6.

[10] D. Lin, P. Zhou, W. N. Fu, S. Stanton, and Z. J. Cendes, “A dynamic core loss model for soft ferromagnetic and power ferrite materials in transient finite element analysis,” *IEEE Trans. Magn.*, vol.40, no.2, Mar. 2004, pp. 1318–1321.